Efficient Blind Image Deblurring Using Nonparametric Regression And Local Pixel Clustering

Yicheng Kang[1], Partha Mukherjee[2], Peihua Qiu[1]

[1] University of Minnesota

[2] Boise State University

Abstract

Blind image deblurring is a challenging ill-posed problem. It would have infinite solutions even in cases when an observed image contains no noise. In reality, the observed image almost always contains noise, and the presence of noise would make the image deblurring problem even more challenging because the noise can cause numerical instability in many existing image deblurring procedures. In this paper, a novel blind image deblurring approach is proposed, which can remove both noise and image blur efficiently without imposing restrictive assumptions on either the point spread function (psf) or the true image. It even allows the psf to be location variant. In the proposed approach, local pixel clustering is used for handling the challenging task of restoring complicated edge structures tapered by blur and nonparametric regression is used for removing noise at the same time. Numerical comparisons with other state-of-the-art image deblurring methods on images with various synthetic and real-life degradations show that our proposed method is capable of handling a wide variety of blurs and works well in applications.

Index Terms: Blind image deblurring, clustering, deconvolution, denoising, edges, image reconstruction, smoothing, surface estimation, nonparametric regression.

1 Introduction

Observed images are not always faithful representations of the scenes that we see. In practice, some degradation often arises in the recording of a digital image. For example, in astronomical imaging, the incoming light in the telescope is often bent by atmospheric turbulence. In aerial reconnaissance, the optical system in camera lens may be out of focus. In daily life, image distortion often arises in cases when there is relative motion between the camera and the object. Among

different degradations, *point degradation* (or, noise) and *spatial degradation* (or, blur) are the most common in practice. Other types of degradations involve chromatic or temporal effects. See Bates and McDonnell (1986) for a detailed discussion about formation and description of various degradations.

In the literature, a commonly used model for describing the relationship between the true image f and its degraded version Z is as follows.

$$Z(x,y) = G\{f\}(x,y) + \varepsilon(x,y), \qquad \text{for } (x,y) \in \Omega, \tag{1}$$

where $G\{f\}(x,y) = \int\int_{R^2} g(u,v;x,y) f(x-u, y-v)\, dudv$ denotes the convolution between a 2-D point spread function (psf) g and a true image intensity function f, $\varepsilon(x,y)$ is the pointwise noise at (x,y), and Ω is the design space of the image. In model (1), it is assumed that the true image f is degraded spatially by g and pointwise by ε, the spatial blur is linear, and the pointwise noise is additive. In most references, it is further assumed that the psf g, which describes the spatial blurring mechanism, is location (or spatially) invariant. That is, $g(u,v;x,y)$ does not depend on (x,y).

Blind image deblurring (BID) is for estimating f from Z when the psf g is not completely specified. This problem is ill-posed in nature because only Z is observed and g, f and ε are all unobservable. So, the number of unknowns is larger than the number of observations. This ill-posed nature would get even worse in cases when g changes over location. In the literature, some image deblurring procedures have been developed under the assumption that the psf g is completely known. Such procedures are referred to be *non-blind*. The main difficulty in non-blind image deblurring has to do with the presence of noise (cf., Qiu 2005, Chapter 7). To overcome the difficulty, a number of image deblurring techniques have been proposed using the regularization framework (e.g., Oliveira *et al.* 2009). In practice, however, it is hard to fully specify the psf g. In cases when the assumed psf is quite different from the true psf, the deblurred image would be seriously distorted. To avoid such limitations, a number of BID methods have been developed. Some of them assume that g follows a parametric model with one or more unknown parameters, and these parameters are estimated together with the true image f by certain algorithms (e.g., Carasso 2001, Carasso 2002, Hall and Qiu 2007a, Joshi and Chaudhuri 2005, Katsaggelos and Lay 1990). Some others assume that the true image f has one or more regions with certain known

edge structures (e.g., Hall and Qiu 2007b, Kundur and Hatzinakos 1998, Qiu 2008, Yang *et al.* 1994). Several BID methods use the Bayesian framework to make the originally ill-posed BID problem well-posed by assuming some prior information on the psf or the true image (e.g., Fergus *et al.* 2006). Some other BID methods estimate both g and f in an alternating fashion, using the iterative Richardson-Lucy scheme (e.g., Biggs and Andrews 1997, Jansson 1997).

This paper proposes an alternative approach to the BID problem. We notice that spatial blur alters the image structure dramatically around step edges (i.e., jumps in f). But the observed image is not affected much by spatial blur at places where f is straight. Based on this observation, our proposed approach pays a special attention to regions around step edges. It consists of two major steps. First, pixels in a neighbourhood of a given pixel are clustered into two groups based on their observed image intensities. At the same time, we make a hypothesis test to check whether the two groups are significantly different from each other. Second, the true image intensity at the given pixel is estimated by a weighted average of the observed image intensities at the pixels in that neighbourhood that belong to the same group as the given pixel. One major feature of this approach is that it does not require any restrictive assumptions on either g or f. It even allows g to vary over location. Numerical comparisons with some representatives of the state-of-the-art image deblurring methods show that the proposed method is capable to handle a wide variety of blurs and it works well in various applications.

The rest part of the article is organized as follows. Our proposed methodology is described in detail in Section 2. Some numerical examples are presented in Section 3. Several remarks conclude the paper in Section 4.

2 Methodology

We describe our proposed BID method in three parts. In Subsection 2.1, our new procedure is described in detail. In Subsection 2.2, a modification to address misclassification in local pixel clustering is discussed. In Subsection 2.3, selection of procedure parameters is discussed.

2.1 Proposed BID Method

Assume that an observed image follows the model

$$Z_{ij} = G\{f\}(x_i, y_j) + \varepsilon_{ij}, \qquad \text{for } i, j = 1, 2, \ldots, n,$$

where $\{(x_i, y_j), i, j = 1, 2, \ldots, n\}$ are equally spaced pixels in the design space $\Omega = [0, 1] \times [0, 1]$, $\{Z_{ij}, i, j = 1, 2, \ldots, n\}$ are observed image intensities, and $\{\varepsilon_{ij}, i, j = 1, 2, \ldots, n\}$ are independent and identically distributed (i.i.d.) random errors with mean 0 and unknown variance σ^2. It is further assumed that f is continuous in Ω except on some edge curves (see Qiu 1998 for a mathematical definition).

For a given pixel $(x, y) \in [h_n, 1-h_n] \times [h_n, 1-h_n]$ where $h_n \in (0, 1/2)$ is a bandwidth parameter, let us consider its circular neighbourhood

$$O(x, y; h_n) = \left\{ (x_i, y_j) \in \Omega : \sqrt{(x_i - x)^2 + (y_j - y)^2} \leq h_n^2 \right\}.$$

In this neighbourhood, a local plane is fitted by the following local linear kernel (LLK) smoothing procedure (cf., Fan and Gijbels 1996):

$$\min_{a,b,c} \left\{ \sum_{i=1}^{n} \sum_{j=1}^{n} \left[Z_{ij} - a - b(x_i - x) - c(y_j - y) \right]^2 K\left(\frac{x_i - x}{h_n}, \frac{y_j - y}{h_n} \right) \right\}, \tag{2}$$

where K is a circularly symmetric bivariate density kernel function with its support on the unit disk. The above LLK smoothing procedure approximates the image intensity surface locally by a plane and uses the kernel function K to control the weights in the weighted least squares procedure (2). Usually, K is chosen such that pixels closer to (x, y) receive more weights, which is intuitively reasonable because pixels closer to (x, y) should provide more information about the image intensity at (x, y). Let $(\widehat{a}(x, y), \widehat{b}(x, y), \widehat{c}(x, y))$ denote the solution to the minimization problem (2). They have the following expression:

$$\widehat{a}(x, y) = \frac{\sum_{i=1}^{n} \sum_{j=1}^{n} w_{ij}^{(1)}(x, y) Z_{ij}}{\sum_{i=1}^{n} \sum_{j=1}^{n} w_{ij}^{(1)}(x, y)}, \tag{3}$$

$$\widehat{b}(x, y) = \frac{\sum_{i=1}^{n} \sum_{j=1}^{n} w_{ij}^{(2)}(x, y) Z_{ij}}{\sum_{i=1}^{n} \sum_{j=1}^{n} w_{ij}^{(2)}(x, y)}, \tag{4}$$

$$\widehat{c}(x, y) = \frac{\sum_{i=1}^{n} \sum_{j=1}^{n} w_{ij}^{(3)}(x, y) Z_{ij}}{\sum_{i=1}^{n} \sum_{j=1}^{n} w_{ij}^{(3)}(x, y)}, \tag{5}$$

where

$$
\begin{aligned}
w_{ij}^{(1)}(x,y) &= [A_{11}(x,y)+A_{12}(x,y)(x_i-x)+A_{13}(x,y)(y_j-y)]K\left(\frac{x_i-x}{h_n},\frac{y_j-y}{h_n}\right),\\
w_{ij}^{(2)}(x,y) &= [A_{21}(x,y)+A_{22}(x,y)(x_i-x)+A_{23}(x,y)(y_j-y)]K\left(\frac{x_i-x}{h_n},\frac{y_j-y}{h_n}\right),\\
w_{ij}^{(3)}(x,y) &= [A_{31}(x,y)+A_{32}(x,y)(x_i-x)+A_{33}(x,y)(y_j-y)]K\left(\frac{x_i-x}{h_n},\frac{y_j-y}{h_n}\right),\\
A_{11}(x,y) &= r_{20}(x,y)r_{02}(x,y)-r_{11}(x,y)r_{11}(x,y),\\
A_{12}(x,y) &= r_{01}(x,y)r_{11}(x,y)-r_{10}(x,y)r_{02}(x,y),\\
A_{13}(x,y) &= r_{10}(x,y)r_{11}(x,y)-r_{01}(x,y)r_{20}(x,y),\\
A_{21}(x,y) &= r_{01}(x,y)r_{11}(x,y)-r_{10}(x,y)r_{02}(x,y),\\
A_{22}(x,y) &= r_{00}(x,y)r_{02}(x,y)-r_{01}(x,y)r_{01}(x,y),\\
A_{23}(x,y) &= r_{01}(x,y)r_{10}(x,y)-r_{00}(x,y)r_{11}(x,y),\\
A_{31}(x,y) &= r_{10}(x,y)r_{11}(x,y)-r_{20}(x,y)r_{01}(x,y),\\
A_{32}(x,y) &= r_{01}(x,y)r_{10}(x,y)-r_{00}(x,y)r_{11}(x,y),\\
A_{33}(x,y) &= r_{00}(x,y)r_{20}(x,y)-r_{10}(x,y)r_{10}(x,y),\\
r_{s_1,s_2}(x,y) &= \sum_{i=1}^{n}\sum_{j=1}^{n}(x_i-x)^{s_1}(y_j-y)^{s_2}K\left(\frac{x_i-x}{h_n},\frac{y_j-y}{h_n}\right),\ \text{for } s_1,s_2=0,1,2,
\end{aligned}
$$

and $\widehat{a}(x,y)$ in (3) is called the LLK estimator of $f(x,y)$. Its weighted residual mean square (WRMS) is defined by

$$
e(x,y)=\frac{\sum_{i=1}^{n}\sum_{j=1}^{n}\left[Z_{ij}-\widehat{a}(x,y)-\widehat{b}(x,y)(x_i-x)-\widehat{c}(x,y)(y_j-y)\right]^2 K\left(\frac{x_i-x}{h_n},\frac{y_j-y}{h_n}\right)}{\sum_{i=1}^{n}\sum_{j=1}^{n}K\left(\frac{x_i-x}{h_n},\frac{y_j-y}{h_n}\right)}. \tag{6}
$$

If (x,y) is in the continuity region of f, then the image structure within $O(x,y;h_n)$ should be approximated well by the local plane described by $(\widehat{a}(x,y),\widehat{b}(x,y),\widehat{c}(x,y))$. Thus, $e(x,y)$ should be relatively small. On the other hand, if $O(x,y;h_n)$ contains edge curves, then the fitted local plane cannot well describe the image structure within $O(x,y;h_n)$. Consequently, the value of $e(x,y)$ would be relatively large. Therefore, $e(x,y)$ can be used to judge whether the neighborhood $O(x,y;h_n)$ contains any edge curves. More specifically, if

$$
e(x,y)>u_n, \tag{7}
$$

then we can conclude that there are edge curves in $O(x, y; h_n)$, where u_n is a threshold value. In such a case, we can cluster the pixels in $O(x, y; h_n)$ into two groups based on their observed image intensities. Intuitively, pixels on the same side of an edge curve have similar intensity values. So, they can be put in the same group. Pixels on different sides of the edge curve have quite different intensity values, and they should be put in different groups. An informative pixel clustering procedure should generate groups such that pixels within a group are similar in their intensity values and pixels in different groups have quite different intensity values. Thus, pixel clustering within $O(x, y; h_n)$ should reflect the local edge structure well without requiring restrictive conditions on the smoothness or shape of the edge curve. In this paper, we suggest using a cut-off constant c to define the two clusters in $O(x, y; h_n)$. More specifically, the two clusters are defined to be

$$\begin{aligned} O_1(x, y; h_n, c) &= \{(x_i, y_j) \in O(x, y; h_n) : Z_{ij} \leq c\}, \\ O_2(x, y; h_n, c) &= \{(x_i, y_j) \in O(x, y; h_n) : Z_{ij} > c\}, \end{aligned}$$

where $c \in R(x, y; h_n)$, and $R(x, y; h_n)$ is the range of the image intensity values in $O(x, y; h_n)$. Namely,

$$R(x, y; h_n) = \left(\min_{(x_i, y_j) \in O(x, y; h_n)} Z_{ij}, \max_{(x_i, y_j) \in O(x, y; h_n)} Z_{ij} \right).$$

So, it is obvious that both $O_1(x, y; h_n, c)$ and $O_2(x, y; h_n, c)$ are non-empty sets for any constant $c \in R(x, y; h_n)$, $O(x, y; h_n, c) = O_1(x, y; h_n, c) \cup O_2(x, y; h_n, c)$, and $O_1(x, y; h_n, c) \cap O_2(x, y; h_n, c) = \emptyset$. Let c_0 be the maximizer to the following maximization problem:

$$\max_{c \in R(x, y; h_n)} \frac{|O_1(x, y; h_n, c)|(\overline{\xi}_1 - \overline{\xi})^2 + |O_2(x, y; h_n, c)|(\overline{\xi}_2 - \overline{\xi})^2}{\sum_{(x_i, y_j) \in O_1(x, y; h_n, c)} (Z_{ij} - \overline{\xi}_1)^2 + \sum_{(x_i, y_j) \in O_2(x, y; h_n, c)} (Z_{ij} - \overline{\xi}_2)^2}, \tag{8}$$

where $|A|$ denotes the number of elements in the pointset A, $\overline{\xi}_s$ denotes the sample mean of the intensity values of the pixels in $O_s(x, y; h_n, c)$, for $s = 1, 2$, and $\overline{\xi}$ denotes the sample mean of the intensity values of all pixels in $O(x, y; h_n, c)$. In (8), the numerator measures the dissimilarity between the two groups, and the denominator measures the dissimilarity of intensity values within each of the two groups. Thus, it is reasonable to cluster the pixels in $O(x, y; h_n, c)$ by maximizing their ratio. It can be checked that (8) is actually the one dimensional version of the clustering criterion proposed by Friedman and Rubin (1967).

Without loss of generality, assume that $(x, y) \in O_1(x, y; h_n, c_0)$. Then, a weighted average of observations in $O_1(x, y; h_n, c_0)$ should provide a good estimate for $f(x, y)$ when there is no blurring

involved, as discussed in the image denoising literature (cf., Qiu 1998). In cases when the observed image contains blur, if the intensity of a pixel is closer to the cut-off constant c_0, then it should receive less weight in the weighted average since it is more likely for that pixel to have blur involved. To address this issue about image blur, besides a bivariate kernel function used in the conventional kernel smoothing procedure to assign more weights to pixels closer to (x, y), a univariate kernel function is used to assign less weights to pixels whose intensity values are closer to c_0. Then, the proposed BID estimator $\widehat{f}(x, y)$ is defined to be the solution to a_0 in the following local constant kernel (LCK) smoothing procedure:

$$\min_{a_0 \in \mathbf{R}} \sum_{(x_i, y_j) \in O_1(x, y; h_n, c_0)} (Z_{ij} - a_0)^2 \, K\left(\frac{x_i - x}{h_n}, \frac{y_j - y}{h_n}\right) L\left(\frac{|Z_{ij} - c_0|}{|Z^{(1)}_{min} - c_0|}\right), \tag{9}$$

where L is a univariate increasing density kernel function with support $[0, 1]$, and $Z^{(1)}_{min}$ denotes the minimum intensity in $O_1(x, y; h_n, c_0)$. It is easy to check that $\widehat{f}(x, y)$ has the following expression:

$$\widehat{f}(x, y) = \frac{\sum_{(x_i, y_j) \in O_1(x, y; h_n, c_0)} Z_{ij} K\left(\frac{x_i - x}{h_n}, \frac{y_j - y}{h_n}\right) L\left(\frac{|Z_{ij} - c_0|}{|Z^{(1)}_{min} - c_0|}\right)}{\sum_{(x_i, y_j) \in O_1(x, y; h_n, c_0)} K\left(\frac{x_i - x}{h_n}, \frac{y_j - y}{h_n}\right) L\left(\frac{|Z_{ij} - c_0|}{|Z^{(1)}_{min} - c_0|}\right)}. \tag{10}$$

In cases when $(x, y) \in O_2(x, y; h_n, c_0)$, $\widehat{f}(x, y)$ can be defined in the same way except that $O_1(x, y; h_n, c_0)$ and $Z^{(1)}_{min}$ in (10) should be replaced by $O_2(x, y; h_n, c_0)$ and $Z^{(2)}_{max}$, respectively, where $Z^{(2)}_{max}$ denotes the maximum intensity in $O_2(x, y; h_n, c_0)$.

To demonstrate the efficacy of the image deblurring procedure (10), a cross section of an image around a step edge, a blurred version, a blurred-and- noisy version and the deblurred version by (10) when K and L are chosen to be the ones used in Section 3 are shown in plots (a)-(d) of Figure 1, respectively. From plot (d), it can be seen that (10) can restore the blurred edge structure to some extent while removing the noise at the same time.

In cases when (7) is not satisfied, it is likely that the pixel (x, y) is in a continuity region of f. In such cases, the spatial blur would not alter the image much, as discussed in Section 1. So, we suggest estimating $f(x, y)$ by the conventional LLK estimator $\widehat{a}(x, y)$ in (3). There are two benefits of doing this. First, it has been well demonstrated in the literature that the LLK estimator has less bias compared to the LCK estimator in continuity regions of f (cf., Fan and Gijbels 1996). Second, since $\widehat{a}(x, y)$ is already computed as a by-product in (7) before we compute $\widehat{f}(x, y)$, it saves

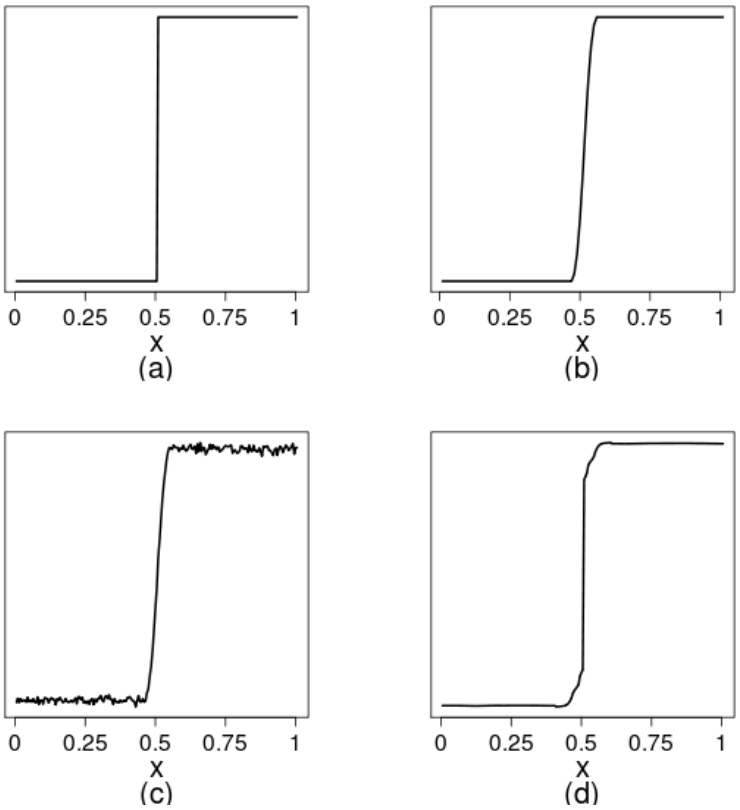

Figure 1: (a): A cross section of an image around a step edge; (b): A blurred version of (a); (c): A blurred-and-noisy version of (a); (d): The deblurred version from (c) by the BID procedure (10).

much computation. By taking into account all these considerations, our proposed BID procedure is summarised below.

Proposed Blind Image Deblurring Procedure

1. For a given pixel (x, y), solve the minimization problem (2) by (3)-(5).
2. Compute the WRMS in (6).
3. If (7) holds, then do local clustering by maximizing (8) and estimate $f(x, y)$ by (10). Otherwise, estimate $f(x, y)$ by (3).

2.2 A Modification

When the noise level of the observed image is quite low, the clustering procedure introduced in the previous subsection works well. However, its misclassification rate would get higher as the observed image gets noisier. As a brief demonstration, let us consider a toy example about an image with a single step edge. A blurred version and a blurred-and-noisy version of this image are shown in Figure 2(a), (b), respectively. The deblurred image by our proposed BID procedure (8)– (10) is presented in Figure 2(c). It can be seen that the step edge structure is restored well and the noise is mostly removed as well. But, the true image intensities of certain pixels around the step edge are not estimated well, which is mainly caused by the misclassification of the clustering procedure. To address this issue, we suggest a modification procedure described below. Assume that (7) holds at a given pixel (x, y). Then, local clustering needs to be performed in $O(x, y; h_n)$ by the clustering procedure discussed in Subsection 2.1 and all the pixels in that neighborhood are grouped into two clusters. If more than four of the eight immediately neighboring pixels of (x, y) are grouped into the same cluster as (x, y), then we say that (x, y) has been correctly classified. Otherwise, we say that (x, y) has been misclassified because (x, y) should belong to the same cluster as most of its immediately neighboring pixels (cf., Figure 3 for a demonstration). The deblurred image of the one presented in Figure 2(b) by the BID procedure (8)–(10) after the modification is shown in Figure 2(d). Compared to Figure 2(c), it can be seen that the misclassification rate has been greatly reduced by the suggested modification.

2.3 Parameter Selection

In the proposed BID procedure (8)–(10), there are two parameters to choose, including the threshold value, u_n in (7) and the bandwidth h_n in (2). To choose a reasonable threshold value u_n, we need to derive the asymptotic distribution of $e(x, y)$ defined in (6). Based on (6), we have

$$
\begin{aligned}
& e(x,y) \\
= \; & \frac{\sum_{(x_i,y_j)\in O(x,y;h_n)} \left[\varepsilon_{ij} + G\{f\}(x_i,y_j) - \widehat{a}(x,y) - \widehat{b}(x,y)(x_i-x) - \widehat{c}(x,y)(y_j-y)\right]^2 K\left(\frac{x_i-x}{h_n}, \frac{y_j-y}{h_n}\right)}{\sum_{(x_i,y_j)\in O(x,y;h_n)} K\left(\frac{x_i-x}{h_n}, \frac{y_j-y}{h_n}\right)} \\
= \; & \frac{\sum_{(x_i,y_j)\in O(x,y;h_n)} \varepsilon_{ij}^2 K\left(\frac{x_i-x}{h_n}, \frac{y_j-y}{h_n}\right)}{\sum_{(x_i,y_j)\in O(x,y;h_n)} K\left(\frac{x_i-x}{h_n}, \frac{y_j-y}{h_n}\right)} +
\end{aligned}
$$

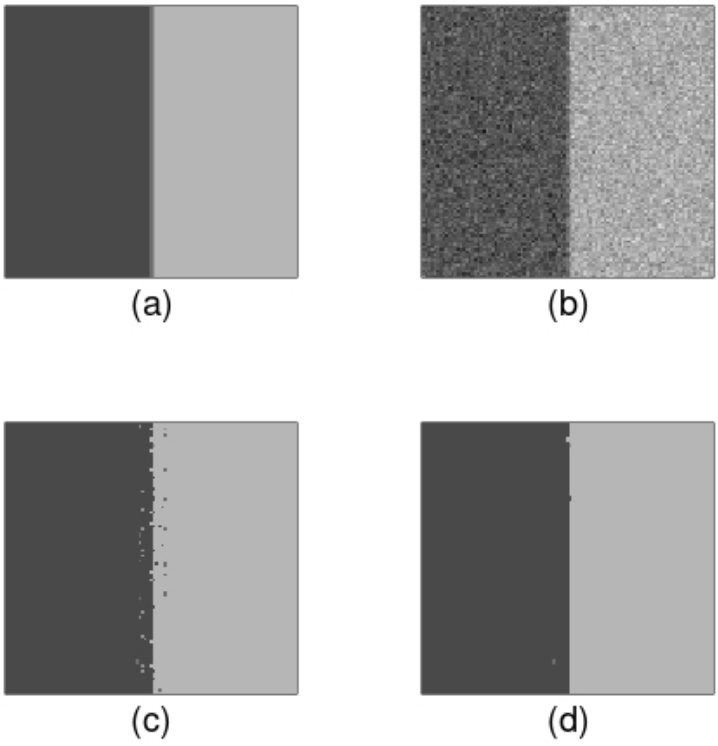

Figure 2: (a): A blurred version of an image with a step edge; (b): A blurred- and-noisy version; (c): The deblurred image by the BID procedure (8)– (10) without the modification; (d): The deblurred image by the BID procedure (8)–(10) with the modification.

$$\begin{aligned} & \frac{2\sum_{(x_i,y_j)\in O(x,y;h_n)} \varepsilon_{ij} \left[G\{f\}(x_i,y_j) - \widehat{a}(x,y) - \widehat{b}(x,y)(x_i-x) - \widehat{c}(x,y)(y_j-y)\right] K\left(\frac{x_i-x}{h_n}, \frac{y_j-y}{h_n}\right)}{\sum_{(x_i,y_j)\in O(x,y;h_n)} K\left(\frac{x_i-x}{h_n}, \frac{y_j-y}{h_n}\right)} + \\ & \frac{\sum_{(x_i,y_j)\in O(x,y;h_n)} \left[G\{f\}(x_i,y_j) - \widehat{a}(x,y) - \widehat{b}(x,y)(x_i-x) - \widehat{c}(x,y)(y_j-y)\right]^2 K\left(\frac{x_i-x}{h_n}, \frac{y_j-y}{h_n}\right)}{\sum_{(x_i,y_j)\in O(x,y;h_n)} K\left(\frac{x_i-x}{h_n}, \frac{y_j-y}{h_n}\right)} + \\ =: \quad & I_1(x,y) + I_2(x,y) + I_3(x,y). \end{aligned}$$

Note that $G\{f\}$ is actually a continuous function. By some arguments similar to those in the proofs of Theorem 2 in Qiu (2009) and Lemma A.1 in Sun and Qiu (2007), it can be checked that both $I_2(x,y)$ and $I_3(x,y)$ converge to zero fast. Also, we notice that $I_1(x,y)$ is a weighted average of i.i.d. random variables $\{\varepsilon_{ij}\}$. By the Central Limit Theorem, $e(x,y)$ has an asymptotic normal

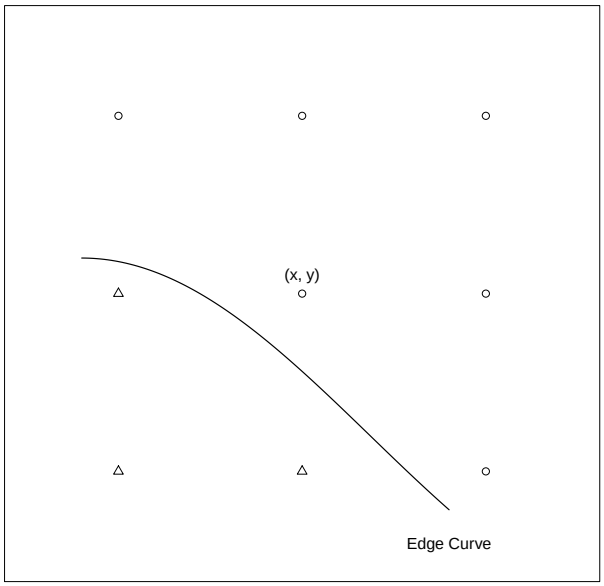

Figure 3: Pixels separated by an edge curve belong to different clusters, which are represented by two different symbols: circles and triangles.

distribution with mean μ_e and variance σ_e^2, where

$$\mu_e = \sigma^2, \qquad \sigma_e^2 = \frac{\left(E(\varepsilon_{11}^4) - \sigma^2\right) \sum_{i=1}^n \sum_{j=1}^n K\left(\frac{x_i - x}{h_n}, \frac{y_j - y}{h_n}\right)^2}{\left[\sum_{i=1}^n \sum_{j=1}^n K\left(\frac{x_i - x}{h_n}, \frac{y_j - y}{h_n}\right)\right]^2}. \tag{11}$$

Therefore, a natural choice of u_n is $\mu_e + \sigma_e Z_{1-\alpha_n/2}$, where $Z_{1-\alpha_n/2}$ is a $(1-\alpha_n/2)^{\text{th}}$ quantile of the standard normal distribution in (11), the significance level α_n needs to be specified beforehand, both $E(\varepsilon_{11}^4)$ and σ^2 are usually unknown in practice. But they can be reasonably estimated using the conventional local kernel smoothing method.

In numerical simulations, the true image is often known. In such cases, h_n can be chosen by minimizing

$$MSE(f, \widehat{f}; h_n) = \frac{1}{n^2} \sum_{i=1}^n \sum_{j=1}^n \left[f(x_i, y_j) - \widehat{f}(x_i, y_j)\right]^2, \tag{12}$$

where $\widehat{f}$ is the deblurred image. In practice, f is usually unknown. In such cases, the cross validation (CV) approach is natural to consider (cf., Qiu 2005, Chapter 2). In the image deblurring problem, however, the mean response is $G\{f\}$, instead of f. In such cases, the CV approach is inappropriate to use because the chosen parameter is for approximating $G\{f\}$. So we suggest

choosing h_n by visual perception of the deblurred image. Note that the choice of h_n is related to the image resolution (i.e., n), the noise level, and the blurring extent (see its definition in Section 3). Based on our numerical experience, when deblurring a typical image with 512×512 pixels by the proposed BID method, it often gives a reasonably good result by choosing h_n between 6/512 and 10/512.

3 Numerical Studies

In this section, we discuss several numerical examples concerning the performance of the proposed BID procedure, denoted as NEW, in comparison with three representative state-of-the-art existing deblurring methods in the literature. The first existing method considered here is the one accomplished by the MATLAB blind deconvolution routine *deconvblind*, which is based on the method discussed by Biggs and Andrews (1997) and Jansson (1997) under the framework of Richardson-Lucy (RL) algorithm. The second existing method is the total variation (TV) image deblurring method proposed by Oliveira *et al.* (2009). The third existing method is the blind image deconvolution procedure developed under the Bayesian framework by Fergus *et al.* (2006). These three existing methods are denoted as RL, TV and Bayes, respectively. It should be pointed out that both RL and Bayes are blind image deblurring schemes, but TV is designed for non-blind image deblurring. Two versions of TV, denoted as TV_1 and TV_2, distinguished by how the psf g is specified, are considered in each numerical example. The specific meanings of TV_1 and TV_2 will be clarified in the context of each example. Throughout this section, the bandwidth h_n used in (2) is chosen by minimizing (12) except in the example of brain image where h_n is chosen by visual perception of the deblurred image, the significance level α_n is fixed at 0.9995, the two dimensional kernel function K used in (2) and (10) is chosen to be $(2/\pi)(1-x^2-y^2)I(x^2+y^2 \le 1)$, and the one dimensional kernel function L used in (10) is chosen to be $(1/1.194958)\exp(x^2/2)I(0 \le x \le 1)$. We choose these two kernel functions because the former is the Epanechnikov kernel function, which is a standard choice in the Statistics literature, and the latter is a truncated Gaussian kernel function, which is commonly used in the Computer Science literature.

In the first example, we consider the Lena test image with 512×512 pixels. The following two

psf's are used:

$$g_1(u,v;x,y) = \begin{cases} \frac{1}{C_1(x,y)} \exp\{-\frac{u^2+v^2}{2}\} I(u^2+v^2 \le 0.1^2) & \text{if } y > 0.5, \\ \delta_0(u)\delta_0(v) & \text{otherwise;} \end{cases}$$

$$g_2(u,v;x,y) = \begin{cases} \frac{1}{C_2(x,y)} I(|u| \le 0.1)\delta_0(v) & \text{if } |x-0.5| \le 0.3 \text{ and } |y-0.5| \le 0.3, \\ \frac{1}{C_2(x,y)} \delta_0(u) I(|v| \le 0.1) & \text{otherwise,} \end{cases}$$

where $C_j(x,y)$ is the standardization constant such that $\int\int_{\mathbf{R}^2} g_j(u,v;x,y)\ dudv = 1$, for any $(x,y) \in \Omega$ and $j = 1, 2$, and $\delta_0(\cdot)$ is the delta function with the point mass at 0. The random noise is generated from the normal distribution $N(0,\sigma^2)$, and two different noise levels, $\sigma = 5$ and 10 are considered. From the above expression, we can see that g_1 is a truncated Gaussian blur for the upper half of the image and there is no blur for the lower half; g_2 is a horizontal motion blur for the central part of the image and is a vertical motion blur for the rest part of the image. Figure 4(a)-(c) present the original Lena image, its blurred version with g_2, and its blurred-and-noisy version with g_2 and $\sigma = 10$, respectively. Figure 4(d)–(h) present the deblurred images by NEW, RL, TV_1, TV_2 and Bayes, respectively, where TV_1 and TV_2 denotes the TV method when the psf is specified as the horizontal motion blur of g_2 and the vertical motion blur of g_2, respectively. It should be pointed out that the support of the psf needs to be specified when using RL and the true support of g_2 is used in this example to show its best performance, and a subregion defined by the coordinates $[86/512, 214/512] \times [293/512, 421/512]$ is prespecified for Bayes, as suggested in Fergus *et al.* (2006) that their algorithm performs better and runs faster if a smaller patch, rich in edge structure, is manually selected. From Figure 4, it can be seen that (i) NEW removes noise and the blur well, (ii) there are many artifacts in the deblurred image of RL and the noise has not been reduced much, and (iii) TV generates many artifacts at places where the psf is misspecified.

Next, we compare the five methods quantitatively. Table 1 presents the values of the root mean squared error (RMSE) defined to be RMSE= $\sqrt{\sum_{i=1}^n \sum_{j=1}^n [f(x_i,y_j) - \widehat{f}(x_i,y_j)]^2/n}$ of the five methods for each case considered based on 100 replicated simulations. The number in each parenthesis represents the standard error of the corresponding RMSE. In cases when the psf is g_1, TV_1 and TV_2 denotes the TV method when the psf is specified as the Gaussian blur of g_1 and a horizontal motion blur, respectively. From Table 1, it can be seen that NEW outperforms all the other four methods. Interestingly, all deblurring methods except the two TV-based methods

Figure 4: (a)–(c): Original Lena image, its blurred version and its blurred-and-noisy version, respectively. (d)–(h): Deblurred images by NEW, RL, TV_1, TV_2 and Bayes, respectively.

perform better as the noise level decreases. But, it turns out that the two TV-based methods perform counter-intuitively the other way. We checked the source code and it seemed that the TV method presented in Oliveira *et al.* (2009) is adaptive in the sense that it does not require users to specify the value of the regularization parameter. In our specific cases when $\sigma = 5$, the TV method automatically chooses the parameter value that does not give a good performance.

Next, we discuss the second numerical example, in which the test image of peppers with 256×256 pixels is used. The psf g considered has the expression:

$$g(u, v; x, y) = \frac{3}{\pi r^2(x, y)} \left(1 - \sqrt{\frac{u^2}{r^2(x, y)} + \frac{v^2}{r^2(x, y)}} \right) I(u^2 + v^2 \leq r^2(x, y)),$$

where $r(x, y) > 0$ may change over location and it is the radius of the circular support of g. In this papers, $r(x, y)$ is called the *blur extent* function. Three blur extent functions, $r_1(x, y) = 0.03(1 - (x - 0.5)^2 - (y - 0.5)^2)$, $r_2(x, y) = 0.03x$, $r_3(x, y) = 0.02$, and two noise levels, $\sigma = 5$, $\sigma = 10$, are considered. Clearly, $r_1(x, y)$ and $r_2(x, y)$, are location variant., and $r_3(x, y)$ is location invariant. In the case with $r_3(x, y)$, the blur described by $g(u, v; x, y)$ is homogeneous across the entire image, which is the case discussed by most references. As in the previous example, the

Table 1: Estimated values of RMSE of the five image deblurring methods in the Lena image example based on 100 replicated simulations. The numbers in the parentheses are the standard errors of RMSE.

	h_1		h_2	
Methods	$\sigma = 5$	$\sigma = 10$	$\sigma = 5$	$\sigma = 10$
New	9.13 (0.01)	9.54 (0.02)	12.09 (0.02)	12.99 (0.03)
RL	19.80 (0.03)	30.73 (0.05)	26.61 (0.04)	29.67 (0.08)
TV_1	295.65 (9.66)	17.11 (0.49)	79.9 (2.02)	26.34 (2.79)
TV_2	185.30 (1.56)	92.24 (4.90)	22.73 (0.22)	14.64 (0.64)
Bayes	26.43 (1.54)	38.11 (1.08)	27.93 (1.11)	40.91 (1.95)

noise is generated from the distribution $N(0, \sigma^2)$. Regarding the five image deblurring methods, we would like to make the following remarks. (i) RL requires the blur extent function to be constant (i.e., location invariant) and completely specified. So, in this example, we searched the value of r to achieve the minimum RMSE such that RL performs the best. (ii) TV requires the psf g to be completely specified and the blur extent function needs to be constant as well. In this example the value of r is searched to achieve the minimum RMSE values for TV_1 and TV_2 as well, where TV_1 and TV_2 denote the TV method when the parametric form of g is correctly specified and when it is misspecified as a horizontal motion blur, respectively. (iii) The prespecified subregion for Bayes is chosen to be $[78/256, 206/256] \times [42/256, 170/256]$.

The results in the same setup as Figure 4 are shown in Figure 5, where the blur extent function $r_2(x, y)$ and $\sigma = 10$ are considered. From the figure, it can be seen that (i) the blur gets more severe when moving from the left side of the image to the right side (cf., plot(b)), (ii) NEW deblurs the image and removes the noise well, (iii) RL performs poorly, (iv) the middle part of the deblurred image by TV_1 looks good but the places near the boundary contain many artifacts because TV cannot handle location variant blur, (v) TV does not work well when the blurring mechanism is misspecified (cf., plot(g)), and (vi) Bayes performs poorly in this example.

In cases when $r_3(x, y)$ (i.e., blur is location invariant) and $\sigma = 10$ are considered, the results are shown in Figure 6. In this case, TV is denoted by TV_1 when the psf is correctly specified and

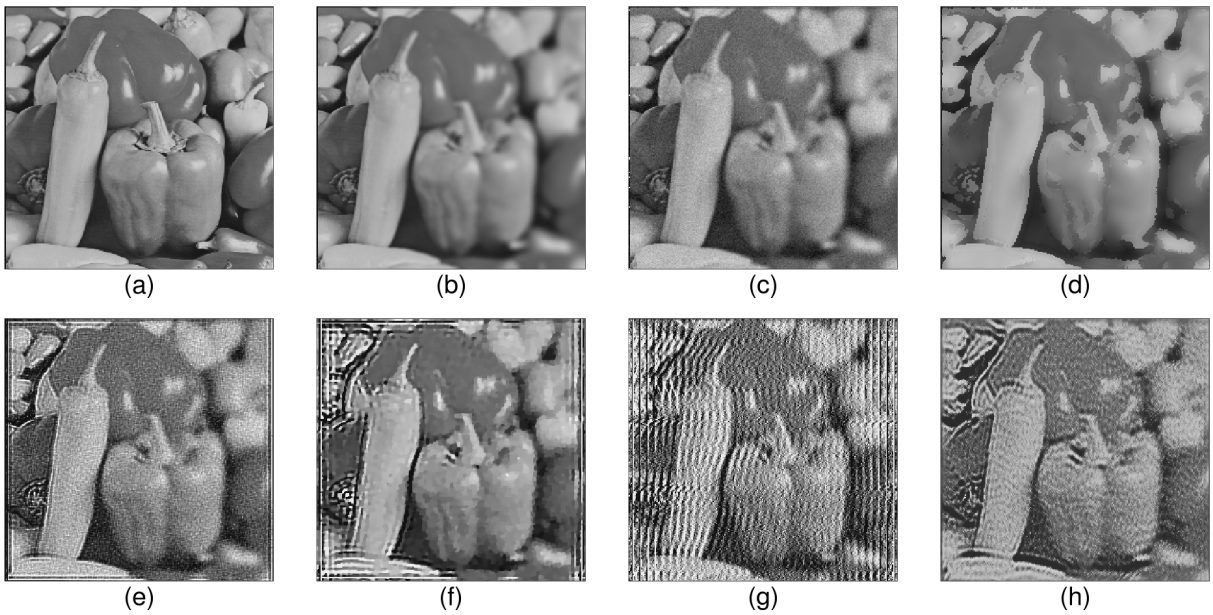

Figure 5: (a)–(c): Original Peppers image, its blurred version and its blurred-and-noisy version, respectively. (d)–(h): Deblurred images by NEW , RL, TV_1, TV_2 and Bayes, respectively.

by TV_2 when the psf is wrongly specified as a horizontal motion blur. From Figure 6, we can see that (i) both RL and Bayes perform poorly, (ii) TV is highly sensitive to the misspecification of the psf, (iii) TV_1 performs well in this case because the psf is location invariant and completely specified, and (iv) NEW still gives a comparable performance to TV_1 despite it uses much less prior information.

The quantitative performance measures of the five methods in the same setup as that of Table 1 are presented in Table 2. It can be seen from Table 2 that (i) NEW outperforms all the other four methods in most cases considered and it works stably as the blur extent function and noise level change, (ii) TV_1 , which requires the parametric form of the psf is correctly specified, works slightly better than NEW in a few cases , and (iii) RL, TV_2 and Bayes all perform poorly.

Finally, we consider an example with a brain test image. Figure 7(a) shows an observed brain image with 217×217 pixels which seems to have some blur involved. Its noisy version is shown in Figure 7(b), where the noise is generated from $N(0, 7^2)$. Figure 7(c)–(f) present the deblurred images by NEW, RL, TV and Bayes, respectively. The bandwidth in NEW is chosen to be $4/217$.

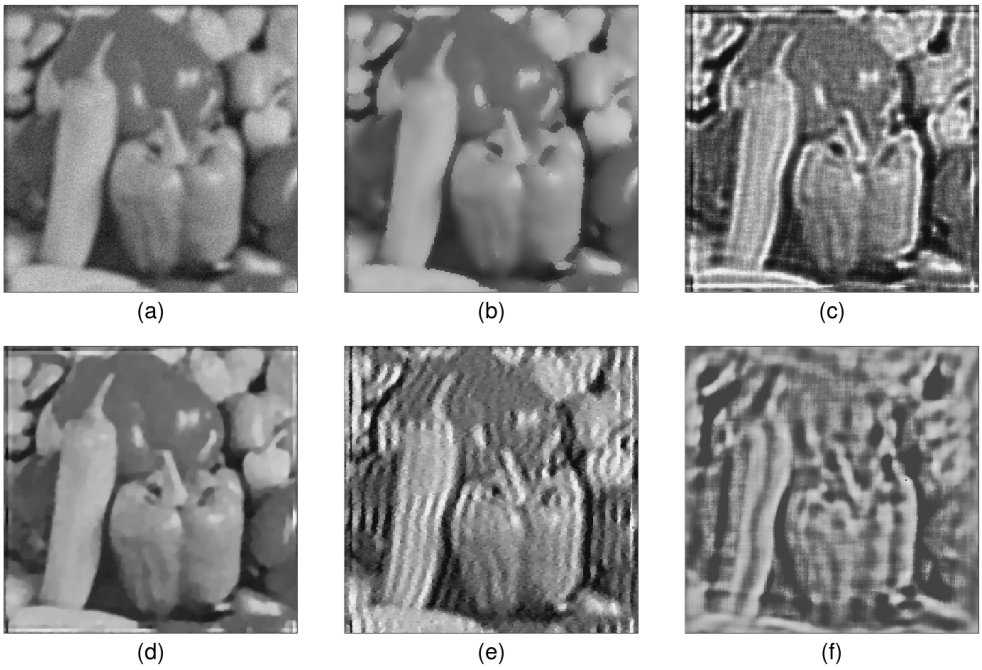

Figure 6: (a) Blurred-and-noisy Peppers image in the case when the blur extent function is $r_3(x, y)$ and $\sigma = 10$. (b)–(f): Deblurred images by NEW, RL, TV_1, TV_2 and Bayes, respectively.

The support of the psf for RL is chosen to give its best visual impression. For TV, the psf is specified as a horizontal motion blur and the blur extent is chosen to give the best visual impression. We also tried several other forms of psf for TV but they did not provide significant improvements. The prespecified subregion required by Bayes is chosen to be $[84/217, 138/217] \times [22/217, 76/217]$. It can be seen from Figure 7 that (i) NEW sharpens the image and removes the noise efficiently, (ii) both RL and Bayes generate many artifacts in their deblurred images around edges, and (iii) the deblurred image by TV does not seem to improve much of the observed image.

4 Concluding Remarks

We have proposed a blind image deblurring method which simultaneously removes spatial blur and pointwise noise from an observed image without imposing restrictive assumptions on the blurring mechanism. It even allows the psf to vary over location. This method is based on our observation that spatial blur alters the image structure significantly around step edges, but does not change

Table 2: Estimated values of RMSE of the five image deblurring methods in the the Peppers image example based on 100 replicated simulations. The numbers in the parentheses are the standard errors of RMSE.

	$r_1(x,y)$		$r_2(x,y)$		$r_3(x,y)$	
Methods	$\sigma = 5$	$\sigma = 10$	$\sigma = 5$	$\sigma = 10$	$\sigma = 5$	$\sigma = 10$
New	18.92 (0.04)	19.78 (0.06)	15.44 (0.05)	16.91 (0.07)	17.27 (0.04)	18.12 (0.06)
RL	27.03 (0.06)	34.73 (0.12)	42.79 (1.46)	47.16 (0.69)	37.91 (0.10)	40.15 (0.18)
TV_1	22.94 (0.09)	19.64 (0.08)	65.37 (0.93)	63.95 (5.98)	26.84 (0.39)	17.76 (0.09)
TV_2	27.71 (0.26)	38.60 (12.02)	76.25 (0.66)	103.17 (1.56)	92.82 (2.13)	62.01 (26.69)
Bayes	29.19 (6.75)	45.05 (3.89)	34.80 (9.00)	43.48 (7.07)	28.28 (10.00)	42.89 (7.68)

image structure much in continuity regions of the image intensity surface. The challenging task of restoring complicated edge structures tapered by blurring is accomplished by a local clustering procedure and by a weighted local smoothing. Numerical comparison with some state-of-the-art image deblurring methods shows that our proposed procedure can do a better job in a wide variety of different blurs and different noise levels.

Our proposed methodology can be generalized in several directions. First, this paper focuses on removing blur around step edges because those places dominate human visual perception. A natural improvement is to properly deblur the observed image around roof/valley edges as well. Moreover, features other than step and roof/valley edges (e.g., peaks, corners, etc.) should also be preserved during image deblurring and denoising. Second, we used a single bandwidth for local smoothing in the current method. The idea of multilevel smoothing that uses variable bandwidths can be incorporated into the proposed method. Third, our method is not fully automatic in the sense that it requires users to choose the bandwidth parameter via visual perception. Automatic bandwidth selection is notoriously difficult in the blind deconvolution problem and it requires much future research.

References

Bates, R.H.T., and McDonnell, M.J. (1986), *Image Restoration and Reconstruction,* Oxford:

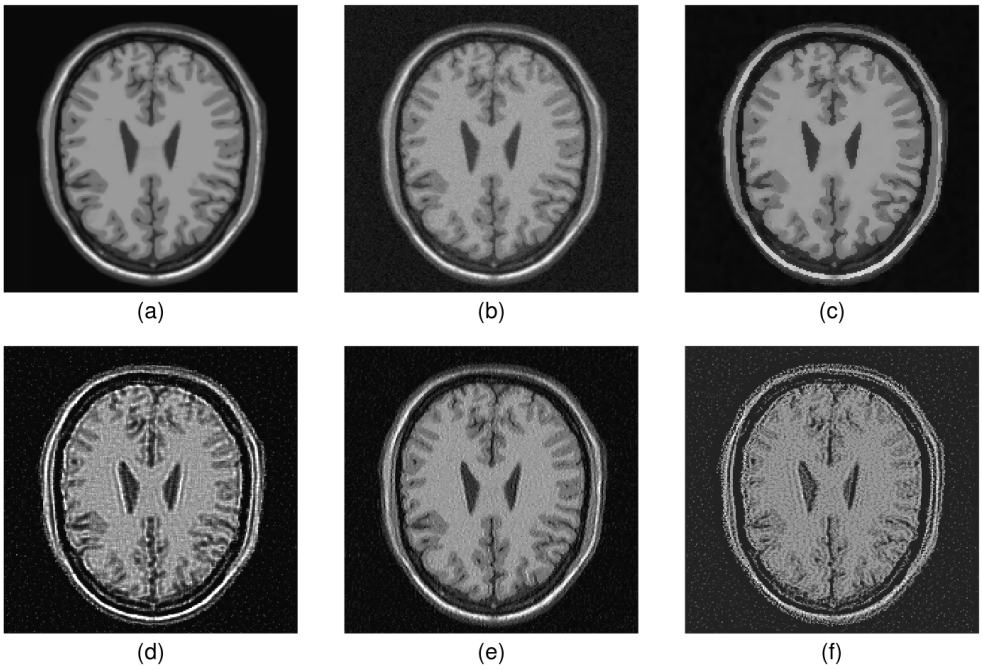

Figure 7: (a): A brain image with some blurring involved. (b): A noisy version of (a). (c)–(f): Deblurred images by NEW, RL, TV and Bayes, respectively.

Clarendon Press.

Biggs, D., and Andrews, M. (1997), "Acceleration of iterative image restoration algorithms," *Applied Optics*, **36, 8**, 1766–1775.

Canny, J. (1986), "A computational approach to edge detection," *IEEE Transactions on Pattern Analysis and Machine Intelligence*, **8**, 679–698.

Carasso, A.S. (2001), "Direct blind deconvolution," *SIAM Journal on Applied Mathematics*, **61**, 1980–2007.

Carasso, A.S. (2002), "The APEX method in image sharpening and the use of low exponent Lévy stable laws," *SIAM Journal on Applied Mathematics*, **63**, 593–618.

Chan, T.F., and Wong, C.K. (1998), "Total variation blind deconvolution," *IEEE Transactions on Image Processing*, **7**, 370–375.

Fan, J., and Gijbels, I. (1996), *Local Polynomial Modelling and Its Applications,* Chapman and

Hall, London.

Fergus, R., Singh, B., Hertzmann, A., Roweis, S. T., and Freeman, W.T. (2006), "Removing Camera Shake From A Single Photograph," *ACM Transactions on Graphics, SIGGRAPH 2006 Conference Proceedings, Boston, MA*, **25, 3**, 787–794.

Figueiredo, M.A.T., and Nowak, R.D. (2003), "An EM algorithm for wavelet-based image restoration," *IEEE Transactions on Image Processing*, **12**, 906–916.

Friedman, H. P. and Rubin, J. (1967) "On some invariant criteria for grouping data," *Journal of the American Statistical Association*, **62**, 1159–1178.

Gonzalez, R.C., and Woods, R.E. (1992), *Digital Image Processing*, Addison-Wesley Publishing Company, Inc.

Hall, P., and Qiu, P. (2007a), "Blind deconvolution and deblurring in image analysis," *Statistica Sinica*, **17**, 1483–1509.

Hall, P., and Qiu, P. (2007b), "Nonparametric estimation of a point spread function in multivariate problems," *The Annals of Statistics*, **35**, 1512–1534.

Jansson, P. A. (1997), *Deconvolution of Images and Spectra*, Academic Press.

Joshi, M.V., and Chaudhuri, S. (2005), "Joint blind restoration and surface recovery in photometric stereo," *Journal of the Optical Society of America, Series A*, **22**, 1066–1076.

Katsaggelos, A.K., and Lay, K.-T. (1990), "Image identification and image restoration based on the expectation-maximization algorithm," *Optical Engineering*, **29**, 436–445.

Kundur, D., and Hatzinakos, D. (1998), " A novel blind deconvolution scheme for image restoration using recursive filtering," *IEEE Transactions on Signal Processing*, **46(2)**, 375–390.

Miskin, J., and MacKay, D.J.C. (2000), "Ensemble Learning for Blind Image Separation and Deconvolution," In *Adv. in Independent Component Analysis*, M. Girolani, Ed. Springer-Verlag.

Oliveira, J.P., Bioucas-Dias, J., and Figueiredo, M. (2009), "Adaptive total variation image deblurring: A majorization-minimization approach," *Signal Processing*, **89**, 1683–1693.

Qiu, P. (1998), "Discontinuous regression surfaces fitting," *The Annals of Statistics*, **26**, 2218–2245.

Qiu, P. (2005), *Image Processing and Jump Regression Analysis,* New York: John Wiley & Sons.

Qiu, P. (2008), "A nonparametric procedure for blind image deblurring," *Computational Statistics and Data Analysis*, **52**, 4828–4841.

Qiu, P. (2009), "Jump-preserving surface reconstruction from noisy data," *Annals of the Institute of Statistical Mathematics*, **61(3)**, 715–751.

Rudin, L.I., Osher, S., and Fatemi, E. (1992), "Nonlinear total variation based noise removal algorithms," *Physica D*, **60**, 259–268.

Skilling, J. (1989, eds), *Maximum Entropy and Bayesian Methods,* Norwell, MA: Kluwer Academic.

Sun J., and Qiu, P. (2007), "Jump detection in regression surfaces using both first-order and second-order derivatives," *Journal of Computational and Graphical Statistics*, **16**, 289–311.

Yang, Y., Galatsanos, N.P., and Stark, H. (1994), "Projection-based blind deconvolution," *Journal of the Optical Society of America A*, **11**, 2401–2409.

You, Y.L., and Kaveh, M. (1996), "A regularization approach to joint blur identification and image restoration," *IEEE Transactions on Image Processing*, **5**, 416–428.